A 2-D Non-local Closure Model for Atmospheric Boundary Layer Simulations

Jiang Weimei (蒋维楣) and *Wang Xuemei* (王雪梅)
Guest Researcher in LAPC, Beijing 100029
Department of Atmospheric Sciences, Nanjing University, Nanjing 210093
Received June 21, 1995; revised August 15, 1995

ABSTRACT

In this paper a new approach for PBL simulation, the non-local closure scheme based on the transient turbulence theory has been used. It was set up as an alternative to local closure schemes which physical concept is reasonable and distinct. A 2-D non-local closure model was developed in order to study the PBL structure and simulate some interesting atmospheric processes over non-uniform underlying surface, especially under the convective and unique weather conditions, such as sea-land circulation and the TIBL structure. The modelled results show good agreement with field measurement.

Key words: Non-local closure, 2-D numerical model, The PBL simulation, Non-uniform underlying surface

I. INTRODUCTION

In non-local closure it is assumed that larger size eddies can transport fluid across finite distance before it mixed with ambient air in vertical by air parcel due to the smaller eddies. This complex diffusion process is called exchange process, in which the physical variable at any point in space may be affected by the variables of any other ones, that is, it is relative to not only the local known variables and their gradient, but also those non-local ones. So it is not suitable to imitate this process by molecular diffusion in which the vertical flux can be parameterized by gradient transport (K) theory.

A simple non-local closure model designed for the daytime convective boundary layer (CBL) was developed by Blackadar (1978), which was the first attempt to use the non-local closure with discrete form in the numerical model. This model has been successfully applied in the mesoscale meteorological model (MM4) to simulate the boundary layer process during the period of free convection (Zhang and Anthes, 1982). The concept of the convective mixing scheme in the model is that convective plume is simulated by mixing material directly from the surface layer to every layer in the CBL. They supposed that upward and downward mixture is symmetric, say, it is from the surface layer to any other levels and symmetrically from there back to the surface layer. In addition the assumption that the downward mixture is identical to the upward which leads to unrealistic transport of material from elevated sources was a main drawback to the model.

In the earlier work of authors (Wang and Jiang, 1993) considering the asymmetry of the atmospheric turbulence transport, a parameterization scheme based on turbulent kinetic energy (TKE) equation has been used. The exchange coefficients between different levels and their effect on other grid points will be different, because of the different energy between upper and lower levels. The research has been conducted incorporating transilient turbulence with 2-D and 3-D mesoscale model. As well as in atmospheric application, the transilient

turbulence theory has been tested in ocean model. In addition, the spectral and eigenvector implication are also being explored by sense (Stull, 1993). In order to study the variations of the PBL structure in temporal and spatial, it is necessary to extend 1–D non–local closure model to a 2–D one. The latter has been applied to the simulations on some interesting atmospheric phenomena occurred over non–uniform underlying surface.

II. MODEL

1. *Conceptual Design of Non–local Closure Scheme*

The transilient theory for non–local turbulence closure was described by Stull (1984), and the 1–D version model was set up in author's paper (Wang and Jiang, 1993). Here it will be summarized briefly.

A new formulation for the transilient coefficients was suggested by Stull (1987). Let $\bar{\xi}$ be some specific properties of the air, such as potential temperature, specific humidity, momentum etc. which are conserved during the vertical movement. To split an air column into N equally–spaced grid boxes, let $\bar{\xi}(t)$ represent the average value of ξ within the grid box j at time t. During time interval Δt, the turbulent mixing may occur between the grid box j and any another grid box i. Provided that C_{ij} represents the proportion of the air coming from box j to all the air in box i. The framework behind non–local mixing is given simply by the matrix multiplication:

$$\bar{\xi}_i(t+\Delta t) = \sum_{j=1}^{N} C_{ij}(t,\Delta t)\bar{\xi}_j(t) \ . \tag{1}$$

As was shown in the prior paper (Wang and Jiang, 1993), the sum of each row of elements in $C_{ij}(0 \leqslant C_{ij} \leqslant 1)$ must equal to unity in order to satisfy the conservation of air mass, so does the sum of each column to satisfy the conservation of property $\bar{\xi}$. The transilient coefficient C_{ij} is given by:

$$C_{ij} = \frac{Y_{ij}}{\| Y \|} \qquad (\text{for} \quad i \neq j) \tag{2a}$$

$$C_{ii} = 1 - \sum_{\substack{j=1 \\ j \neq i}} C_{ij} \ . \tag{2b}$$

where N denotes the number of grid points, $\| Y \|$ is scalar norm of the matrix (Y):

$$\| Y \| = \mathrm{Max}\left(\sum_{j=1}^{N} Y_{ij} \right) \tag{3}$$

here Y_{ij} is used to describe a "mixing potential" between any two adjacent grid–boxes i and j and it is a symmetric matrix, that is $Y_{ij} = Y_{ji}$. The mixing potential depends on the unstability in air stratification and is contained in the TKE equation. Using the normalized TKE equation for the parameterization of Y_{ij} gives finally:

$$Y_{ij} = \frac{\Delta t T}{(\Delta_{ij} Z)^2}\left[(\Delta_{ij}\bar{u})^2 + (\Delta_{ij}\bar{v})^2 - \frac{g(\Delta_{ij}\bar{\theta})(\Delta_{ij} Z)}{\bar{\theta} Ri_c} \right] - \frac{D\Delta t}{T} \ , \quad (i \neq j) \tag{4}$$

where Δt is integral time step; T is time scale of turbulence mixing; D is dimensionless

dissipation factor; Ri_c is dimensionless parameter named critical Richardson number; $\Delta_{ij}Z$ denotes the grid spacing between grid-boxes i and j. This is for the case of $i \neq j$. When $i = j$, Y_{ij} is characterized as the internal mixing in the box.

Some results from the PBL field experiments demonstrated that the internal mixing is always larger than the mixing between the boxes. So a reference potential Y_{ref} is defined to account for the mixing potential within the box i. This reference potential should be independent of time step and grid size. According to the sensitivity study, Stull (1987) suggested $Y_{\text{ref}} = 1000$ to be the correct order of magnitude. And typical value of $Y_{i,i+1}$ varies from 3000 for strong convective turbulence to 20 for weak nocturnal turbulence. Thus the final parameterization for internal mixing potential is:

$$Y_{ij} = \text{Max}(Y_{i,i+1}, Y_{i,i-1}) + Y_{\text{ref}} \quad . \tag{5}$$

The approach outlined above is a strongly parameterized version in which freedom degrees change from $(N^2 - N)$ to 4, where four parameters are $T; D; R_{i_c}$ and Y_{ref}.

2. *Parameterization and Model Discretization*

The 1-D model was used in every spaced grid point in the vertical direction. A variety of domain size (300—3000 m), grid spacings ($\Delta z = 10$—500 m) and time step increments ($\Delta t = 5$—30 min) may be used in the simulation. There are no numerical stability limitations on the relationship between Δz and Δt, so the model is absolutely numerically stable.

Based on the air mass conservation equation, the transport between the grid-boxes can be calculated from the matrix Y and the turbulent kinematic flux $\overline{w'\xi'(k)}$. $\overline{w'\xi'(k)}$ denotes the flux at the top of the grid-box k which was diagnosed from:

$$\overline{w'\xi'(k)} = \frac{\Delta z}{\Delta t} \sum_{j=1}^{k} \sum_{i=1}^{N} C_{ij} (\bar{\xi}_i - \bar{\xi}_j) \tag{6}$$

for the turbulence flux is zero at the solid boundary, Eq.(6) can be re-expressed as a recursion relation to save computation time

$$\overline{w'\xi'(k)} = \overline{w'\xi'(k-1)} + \frac{\Delta z}{\Delta t} \sum_{j=1}^{N} C_{kj} (\bar{\xi}_k - \bar{\xi}_j) \tag{7}$$

and

$$\overline{w'\xi'(k)} \quad |_{k=0} = 0 \quad .$$

3. *Two-Dimensional Model*

(1) *Treatment schemes*

In order to analyze the variations of some physical properties of the air in temporal and spatial more apprehensively, it is very necessary to extend 1-D model to 2-D one. In 2-D model, following treatments should be included: (1) the non-uniform exchange coefficient was used to treat the turbulent transport process; (2) for the horizontal grid spacing is considerably larger than that of in vertical, the effect of horizontal advection is much stronger than that of the horizontal diffusion. So in the non-local closure scheme merely the vertical non-local turbulent exchange process is to be taken into account; (3) due to the existence of the inversion, the depth of the atmospheric boundary layer may decrease to just one vertical grid spacing. In such case using the gradient transport (K) theory is more reasonable than use

of non-local closure scheme which can deal successfully with the daytime CBL.

(2) *Governing equations*

In Cartesian coordinate system, Y-axis is along the shoreline while x-axis directs to inland and z-axis is toward vertical upward. The shoreline is supposed straight and unlimited so the distribution is horizontally homogeneous along the shoreline and the hydrostatic assumption can be satisfied. Considering a horizontally homogeneous and incompressible flow, an Exner function π is introduced into model (Pielke, 1984). Based on the definition of the potential temperature and the hydrostatic equilibrium state equation for ideal gases, the term of horizontal pressure gradient in motion equation can be re-written: $\frac{\partial p}{\partial z} = -\rho g$. Then a set of governing equations for 2-D model is given as follows:

$$\frac{\partial u}{\partial t} + u\frac{\partial u}{\partial x} + w\frac{\partial u}{\partial z} = fv - \theta\frac{\partial \pi}{\partial x} + K_H\frac{\partial^2 u}{\partial x^2} - \frac{\partial}{\partial z}\overline{(w'u')} , \tag{8}$$

$$\frac{\partial v}{\partial t} + u\frac{\partial v}{\partial x} + w\frac{\partial v}{\partial z} = -fu + K_H\frac{\partial^2 u}{\partial x^2} - \frac{\partial}{\partial z}\overline{(w'v')} . \tag{9}$$

$$\frac{\partial \theta}{\partial t} + u\frac{\partial \theta}{\partial x} + w\frac{\partial \theta}{\partial z} = K_H\frac{\partial^2 \theta}{\partial x^2} - \frac{\partial}{\partial z}\overline{(w'v')} , \tag{10}$$

$$\frac{\partial u}{\partial x} + \frac{\partial w}{\partial z} = 0 , \tag{11}$$

$$\frac{\partial \pi}{\partial z} = -\frac{g}{\theta} , \tag{12}$$

$$\frac{\partial \bar{e}}{\partial t} + u\frac{\partial \bar{e}}{\partial x} + w\frac{\partial \bar{e}}{\partial z} = K_H\frac{\partial^2 \bar{e}}{\partial x^2} - \overline{w'u'}\frac{\partial u}{\partial z} - \overline{w'v'}\frac{\partial v}{\partial z} + \frac{g}{\theta_0}\overline{w'\theta'} - \varepsilon , \tag{13}$$

$$\frac{\partial \overline{u'^2}}{\partial t} + u\frac{\partial \overline{u'^2}}{\partial x} + w\frac{\partial \overline{u'^2}}{\partial z} = K_H\frac{\partial^2 \overline{u'^2}}{\partial x^2} - 2\overline{u'w'}\frac{\partial u}{\partial z} - \frac{(2\bar{e})^{1/2}}{3l_1}\left(\overline{u'^2} - \frac{2\bar{e}}{3}\right) - \frac{\varepsilon}{3} , \tag{14}$$

$$\frac{\partial \overline{v'^2}}{\partial t} + u\frac{\partial \overline{v'^2}}{\partial x} + w\frac{\partial \overline{v'^2}}{\partial z} = K_H\frac{\partial^2 \overline{v'^2}}{\partial x^2} - 2\overline{w'v'}\frac{\partial v}{\partial z} - \frac{(2\bar{e})^{1/2}}{3l_1}\left(\overline{v'^2} - \frac{2\bar{e}}{3}\right) - \frac{\varepsilon}{3} , \tag{15}$$

$$\frac{\partial \overline{w'^2}}{\partial t} + u\frac{\partial \overline{w'^2}}{\partial x} + w\frac{\partial \overline{w'^2}}{\partial z} = K_H\frac{\partial^2 \overline{w'^2}}{\partial x^2} + 2\frac{g}{\theta}\overline{w'\theta'} - \frac{(2\bar{e})^{1/2}}{3l_1}\left(\overline{w'^2} - \frac{2\bar{e}}{3}\right) - \frac{\varepsilon}{3} . \tag{16}$$

Where $(l_1, l_2) = (A_1 l, A_2 l)$ and it takes form as:

$$l = \begin{cases} 0.4\ z & \text{for } z \leqslant 200\ \text{m} \\ 70\ \text{m} & \text{for } z > 200\ \text{m} \end{cases}$$

$$A_1 = A_2 = 0.78 , \quad \varepsilon = e^{3/2} / \Lambda_1 , \quad \Lambda_1 = 15l ,$$

the horizontal turbulence exchange coefficient K_H is a constant (50 $m^2 s^{-1}$) (McNider, 1981; McNider and Pielke, 1981).

In order to close the system of governing equations, the second momentum was parameterized as follows: under the noctural stable stratification condition first order closure based on the gradient transport (K) theory was used, while under the day time convective unstable condition, as mentioned above, the utilization of non-local closure scheme is suitable.

(3) *Model domain, boundary and initial conditions*

The total height of model layer is 2240 m. It is then divided into two layers: surface layer which depth is 10 m and intermediate layer. The horizontal domain is 60 km in which 20 km is on water surface and 40 km on land surface. The grid spacing is $\Delta x = 2$ km in horizontal and $\Delta z = 80$ m in vertical. At the bottom boundary it is assumed that (1) the wind speed at surface is zero; (2) the temperature is constant on the water surface and horizontally uniform on the ground surface. The temperature varies on the ground surface in form of sine curve, which begins to increase at 08: 00 and attains the peak value at 14: 00. On the top boundary, all of variables are supposed constant. On the lateral boundary, it is assumed that $\frac{\partial}{\partial x}(u,v,\theta) = 0$, $w = 0$ and the hydrostatic equilibrium assumption is satisfied. The initial conditions are as follows: the initial wind field $u = u_g = 3$ m/s, $v = v_g = 0, w = 0$. The second order momentum $\overline{u'^2}$, $\overline{v'^2}$, $\overline{w'^2}$ are equal to 2×10^{-5} m^2/s^2. $\overline{w'u'}, \overline{w'v'}, \overline{w'\theta'} = 0$; $P(z = z_0) = 1013.5$ hPa; Z_0 denotes the roughness length on the surface; $\theta(z = z_0) = \theta_0$; $\theta(z) = \theta_0 + 0.07z$, $\theta_0 = 281.5$ K, $A = 7.1$°C; $T_0 = 86400$ s.

III. NUMERICAL TESTS AND SIMULATION ANALYSIS

1. *Sensitivity Tests for Model Parameters*

As mentioned above, there are four main parameters: T, D, Ri_c, Y_{ref} in the 2–D non–local closure model. The sensitivity tests for these parameters under daytime convective condition have been executed to study the effect of parameters on model results. Based on the previous work (Wang and Jiang, 1993) basic values such as $Ri_c = 0.21, T = 1000$ s, $D = 1$, $Y_{ref} = 1000$ were used in the model. The test results presented in Fig. 1 (A, B, C, D) show the vertical distributions of turbulent fluxes $\overline{w'u'}, \overline{w'\theta'}, \overline{u'u'}$ and TKE for different turbulence time scales $T = 1000$ s, 100 s, 10 s. It can be seen in the figure that $T = 1000$ s is suitable timescale to be used in the model because in $T = 1000$ s case convective motion become stronger and the entrainment process will occur on the top of boundary layer. These phenomena are in accord with the results from the field experiments (Clarke, 1971; Wang and Jiang, 1993). Some tests for other parameters have been executed also and the test results will not be presented here owing to the limitation of space.

In general, the non–local closure model is more sensitive to turbulent time scale T than other parameters, while the model sensitivity to Ri_c is obvious either. The variation of D in certain range has no obvious effect on model, meanwhile the sensitivity to Y_{ref} is lowest. In order to determine the suitable values for the model parameters, the data from Qinhuangdao PBL field experiment (Jiang et al., 1991) were used to check the correctness of these parameters.

2. *Tests Under the Ideal Condition on the Thermal Internal Boundary Layer (TIBL)*

Using the 2–D model and parameters related above, a calibrated simulation was made under following experimental conditions: $u_g = 3$ m/s, $V_g = 0$ and it was typical onshore flow case. Initial air stratification was stable $\left(\frac{\Delta\theta}{\Delta z}\right) = 7.0 \times 10^{-3}$ K/m on the water surface). A 40 km (in x) × 3 km (in z) domain was used for all runs and the $\Delta z = 80$ m, $\Delta x = 2$ km.

The simulation started at 08: 00 L.S.T. and ended after 10 h. The time step was $\Delta t = 36$ s. The hourly output of the simulation included the distributions of $\theta, u, w, \overline{w'u'}, \overline{w'\theta'}, \overline{u'^2}, \overline{w'^2}$ and TKE etc.

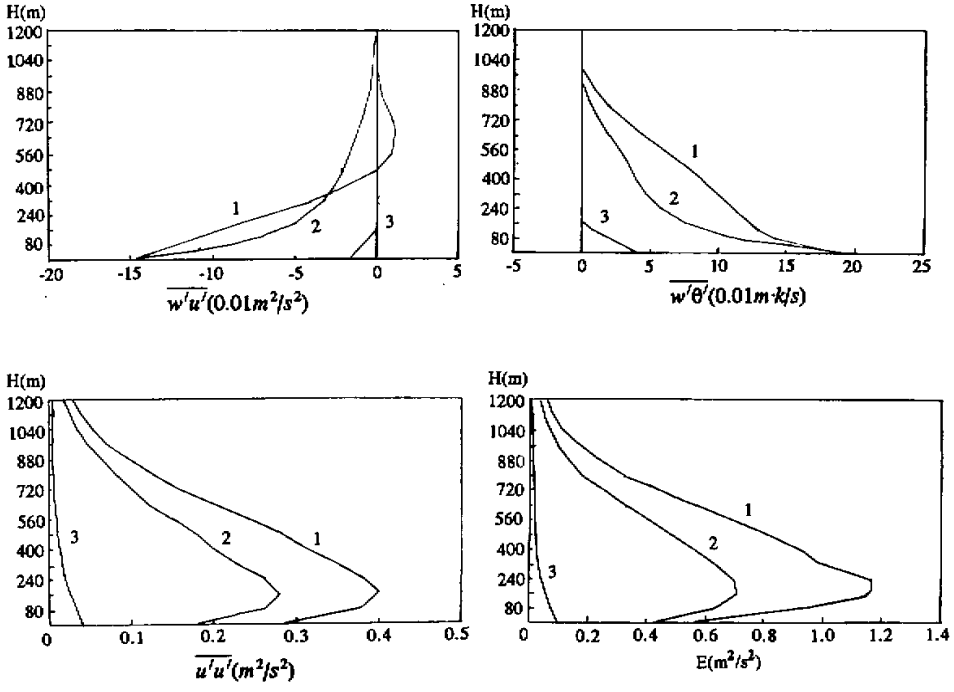

Fig. 1. Distributions of the turbulent characteristic variables in different turbulence time scales T (curve 1: T = 1000 s; 2: T = 100 s; 3: T = 10 s). (A) $\overline{w'u'}$; (B) $\overline{w'\theta'}$; (C) $\overline{u'u'}$; (D) TKE.

Fig. 2 (A, B, C, D) presents the simulation results for potential temperature field at different time, from which the difference between thermal features of the mixing layer over land and water is displayed. And then the TIBL on shore can be clearly identified from the simulation results. During the temperature increasing period on ground surface, there is an unstable stratification over land and it extends toward inland as well as upward gradually. It is obvious that the appearance of the unstable zone is the results of heating of the underlying surface on land and it is also relative to the temperature difference between ground surface and water surface in coastal area. So the TIBL height can be identified by the boundary of this unstable zone.

In Fig. 3 (A, B, C, D) the distributions of the wind speed (u) along x axis are showed. It demonstrates that the centres of high value and low value appear over the intermediate zone located between water and land surface and the low center is over the high one. A vertical circulation was formed in the TIBL because of the uniform heating on the underlying surface. At 14:00 L.S.T. the heating on ground surface is the strongest and the sea breeze comes to maturity and is the strongest either. At this time the depth of the unstable zone is highest, about 300 m, and extends farthest toward inland. The depth of the offshore flow layer is about 960 m and 2–3 times deeper than that of onshore flow layer. This is in accord with observed result.

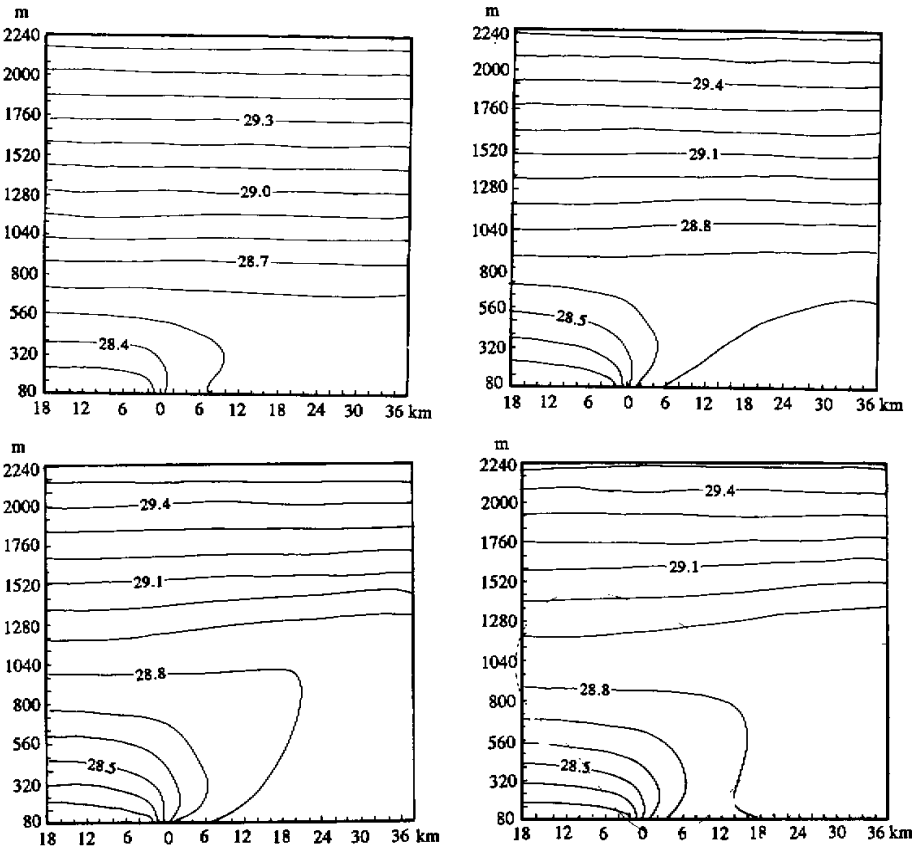

Fig. 2. Distributions of the potential temperature θ (A) 10:00; (B) 12:00 (C) 14:00; (D) 16:00 In figures: 2,3 and 12–17, the lateral scale is distance from shoreline and the vertical scale is height.

Generally speaking, when the prevailing wind is not strong enough, a complete and clear local sea breeze circulation will occur. This is in accord with observed result.

The model can be used to obtain the distributions of the variances of velocity components $\overline{u'^2}$, $\overline{v'^2}$, $\overline{w'^2}$. The high value center of the variance is usually at low altitude. It is due to additional turbulence caused by surface vertical friction in $\overline{u'^2}$ and the strong thermal convection over there caused by heating on the ground surface in $\overline{w'^2}$. The vertical profiles of $\overline{u'^2}$, $\overline{v'^2}$, $\overline{w'^2}$ at different downwind distanes can also be obtained from the computed fields and shown in Figs. 4–6. At the time 14:00 L.S.T. the turbulent activity in sea breeze intermediate zone is more vigorous than in inland area far from the shore. There is a regular pattern of $\overline{w'^2} > \overline{u'^2} > \overline{v'^2}$ under the layer of 500 m and $\overline{w'^2} > \overline{v'^2} \approx \overline{u'^2}$ over 500 m. All of these is conversant with the general features on turbulent structure in CBL.

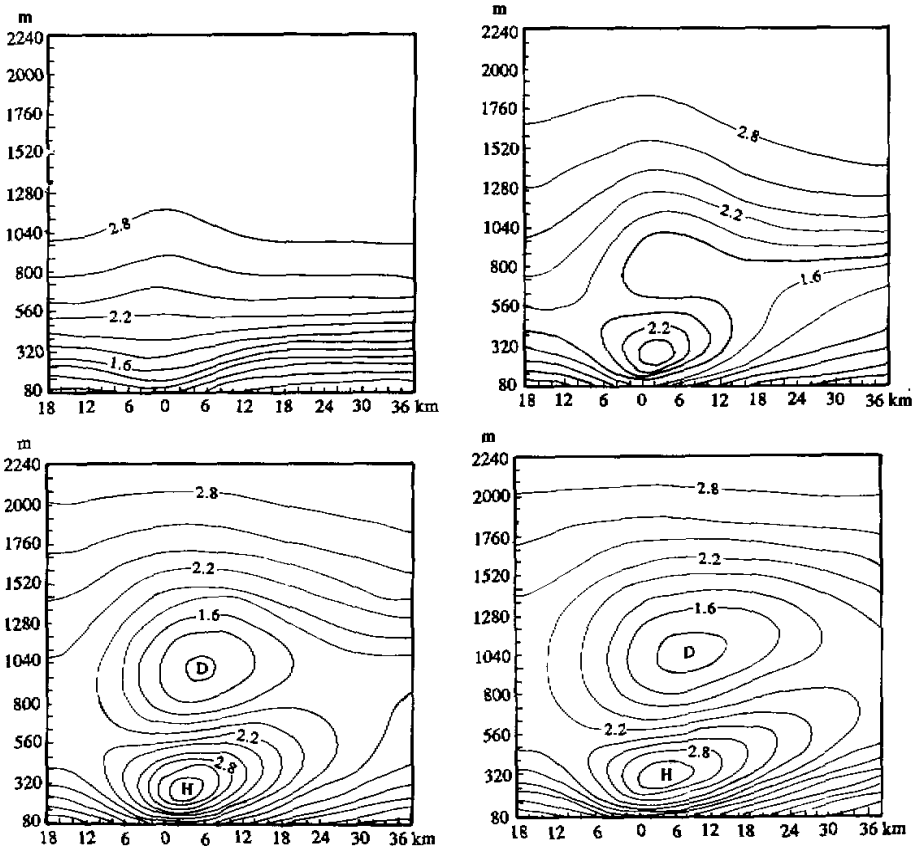

Fig. 3. Distributions of the mean wind speed u (A) 10:00; (B) 12:00; (C) 14:00 (D) 16:00.

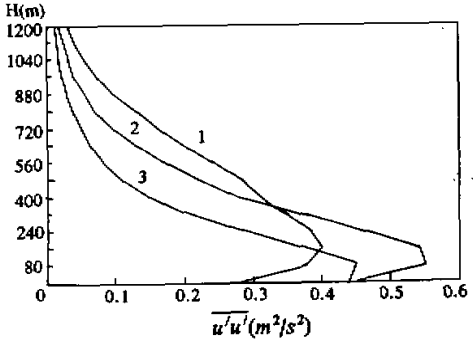

Fig. 4. Profiles of the $\overline{u'^2}$ at different downwind distances (curve 1: x = 20 km; 2: x = 6 km; 3: x = 2 km).

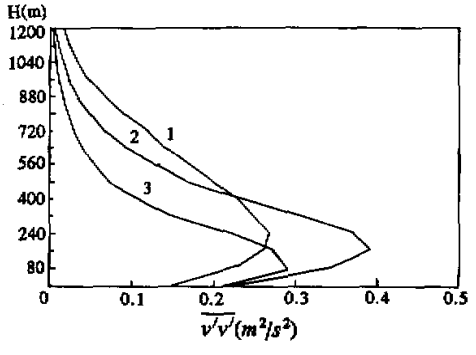

Fig. 5. Profiles of the $\overline{v'^2}$ at different downwind distances (curve 1: x = 20 km; 2: x = 6 km; 3: x = 2 km).

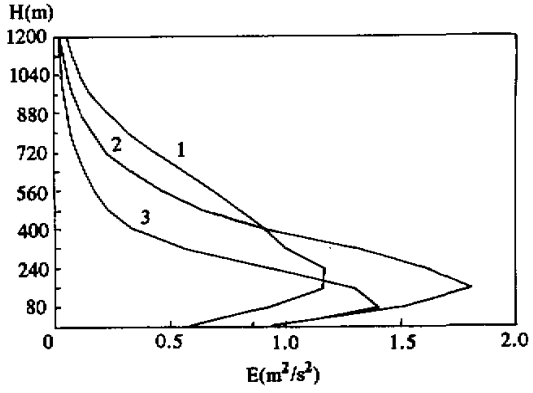

Fig. 6. Profiles of the $\overline{w'^2}$ at different downwind distances (curve 1: x = 20 km; 2: x = 6 km; 3: x = 2 km).

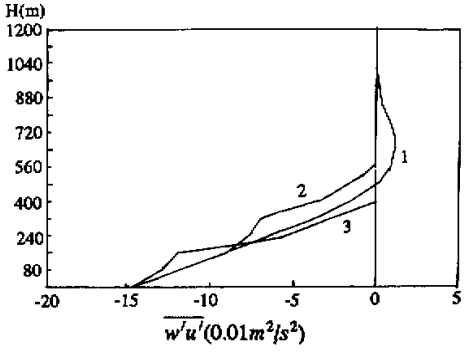

Fig. 7. Profiles of the $\overline{w'u'}$ at different downwind distances (curve 1: x = 20 km; 2: x = 6 km; 3: x = 2 km).

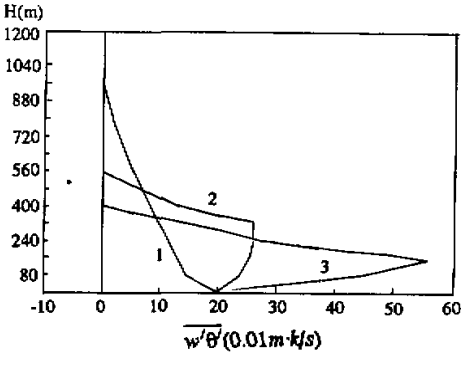

Fig. 8. Profiles of the $\overline{w'\theta'}$ at different downwind distances (curve 1: x = 20 km; 2: x = 6 km; 3: x = 2 km).

Fig. 7 and Fig. 8 present the profiles of the fluxes $\overline{w'u'}$ and $\overline{w'\theta'}$ at different downstream positions. In Fig. 8 the profiles 2 and 3 are posited in the intermediate zone and there exist maximum values of $\overline{w'\theta}$ at the lower level. These are caused mainly by the sea breeze front moving forward. In inland mixing layer (x = 20 km) $\overline{w'\theta'}$ is on the decrease with the increasing height. The negative fluxes occur on the top of layer owing to the entrainment process and are in good agreement with the distributions of the fluxes in CBL. Fig. 9 gives the distributions of turbulent kinetic energy (TKE) at the different distances. At the points 6 km far from shoreline near surface the turbulent energy is on the increasing because of the stronger vertical shear caused by the invading of sea breeze front and on the decrease with the increasing altitude. When distance from shoreline is 20 km, the turbulent energy in the surface layer becomes weak and the lapse rate with the altitude is smaller than that of the first case.

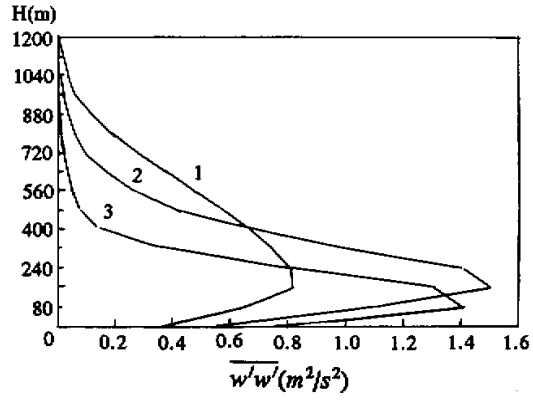

Fig. 9. Profiles of the TKE at different downwind distances (curve 1: x = 20 km; 2: x = 6 km; 3: x = 2 km).

These factors characterize sufficiently that turbulence features are different between the intermediate zone and inland mixing layer.

3. *Simulation Scenario*

Simulations on real cases presented here are parts of those on PBL over coastal area based on data taken from a PBL field experiment in Qinhuangdao area which is located in the coastal area of the Northern China at 39°56′N and 119°36′E. A domain (40 × 24 km) is used for all simulations. Fig. 10 shows the domain, grid mesh and some observation stations. On the simulation day the synoptic situation over the region was relatively stable with typical uniform pressure pattern and without any special synoptic process. In lower layer the wind speed was less than 3 m / s. The background synoptic flow system was favourable for the developing sea breeze and the sea breeze circulation characteristics were typical. Starting from 08:00 L.S.T., the numerical integration was proceeded up to 08:00. Initial fields of the wind and temperature obtained from the observation stations were posited 1.5 km and 4.4 km from shoreline.

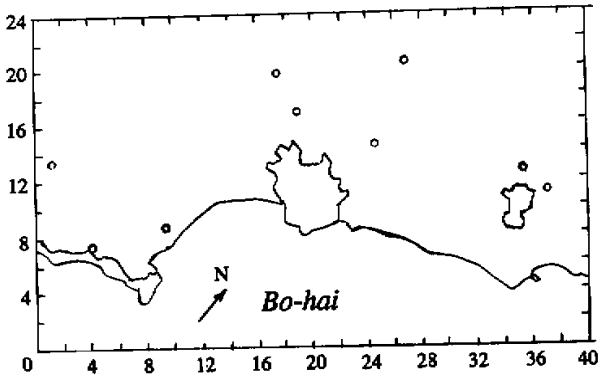

Fig. 10. Simulation domain and computation grid mesh.

During 04:00 to 08:00 there was land breeze with offshore flow pattern obviously below 300 m and a radiation inversion layer with the depth of about 100 m. During 0 5:00–07:00 in the early morning, before the model running, the land breeze began to transform into the sea breeze. There was a transition period from a land breeze to a sea breeze, then the sea breeze becomes dominant in the period of 08:00–09:00. The observed depth of the circulation layer was about 550 m at a station about 4500 m far from shoreline during 10:00–11:00. After that the sea breeze maintained until 18:00~19:00. Then the sea breeze began to subside and switched to a land breeze again. During the thickness of the sea breeze flow–layer period, the top boundary of the return flow layer (IBL) increased linearly with time and onshore distance from the sea breeze front.

In order to know the specific spatial and temporal distributions of both mean and turbulent PBL flow fields, a comparison between simulated and observed results was made and the results are shown in Fig. 11.

Figs. 12 and 13 present the simulated fields of onshore flow in u,w at 14:00. As described above, at 14:00 the sea breeze was on the increasing and pushing inland. Its front can be seen clearly in the PBL field. At 16:00 the sea breeze extends inland, continually.

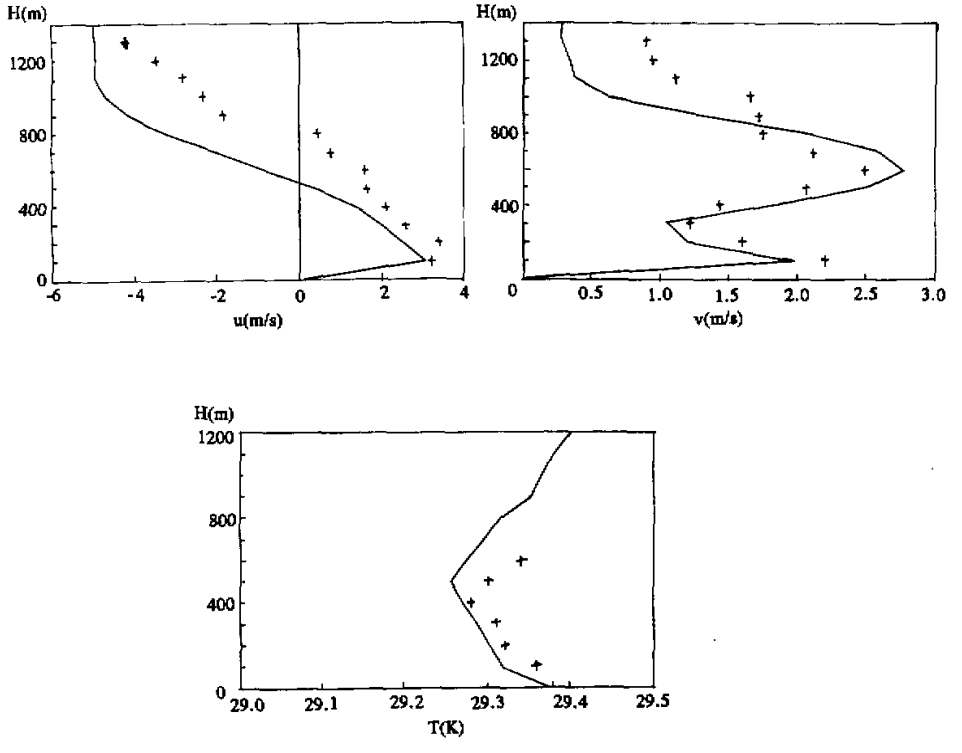

Fig. 11. Profiles of the potential temperature θ (solid curve: computed; point curve: observed).

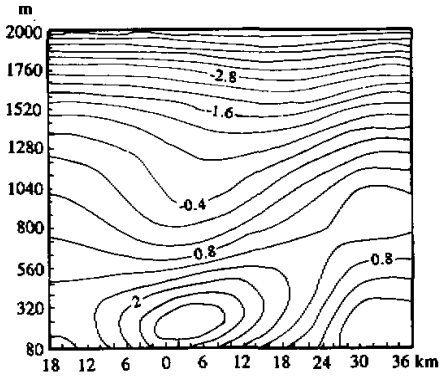

Fig. 12. Distribution of the u at 14:00.

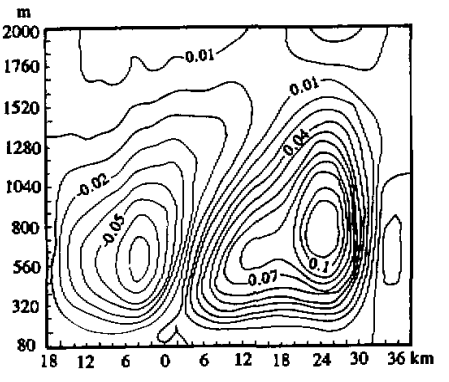

Fig. 13. Distribytion of the w at 14:00.

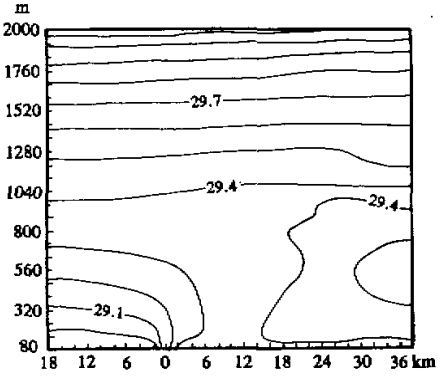

Fig. 14. Distribution of the θ at 14:00.

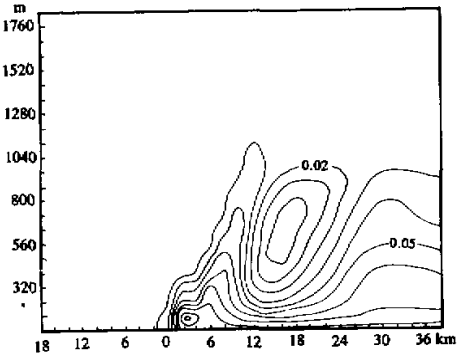

Fig. 15. Distribution of the $\overline{w'u'}$ at 14:00.

Fig. 14 shows the simulated results of θ field. The figure indicates different thermal features between the mixing layer inland and the TIBL on shoreline area. The sea breeze flow extended continuously upward and to inland, the depth of the TIBL is about 500 m. Figs. 15 to 17 present the fields of the $\overline{w'u'}$, $\overline{w'\theta'}$ and TKE(e). Air motion is stable and in the Fig. 15 it can be seen that at 10:00 the momentum fluxes $\overline{w'u'}$ is small and it exists just near ground surface. At 14:00 sea breeze, the turbulent intensities characterized by $\overline{u'^2}$, $\overline{v'^2}$,$\overline{w'^2}$ and TKE are all on the increasing. The entrainment occurred at the upper part of the profile of fluxes $\overline{w'u'}$,$\overline{w'\theta'}$ and the high value center of the turbulent energy and the maximum appeared both at 14:00 while a high value center appeared at higher levels which is caused by the wind shear on those levels. At 16:00 the turbulent energy began to decrease.

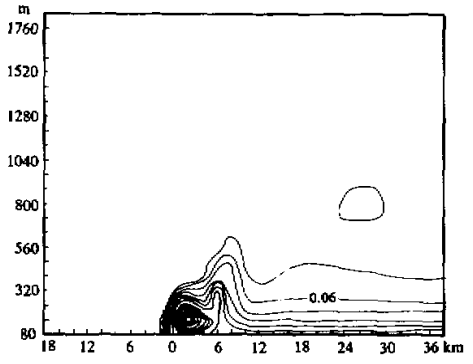

Fig. 16. Distribution of the $\overline{w'\theta'}$ at 14:00.

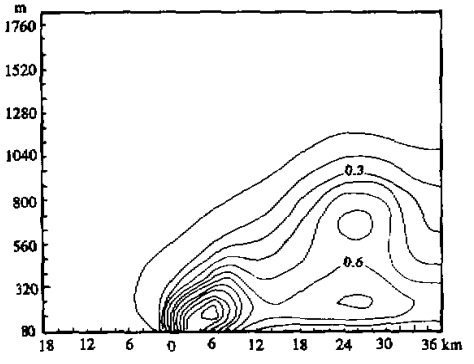

Fig. 17. Distribution of the TKE at 14:00.

IV. DISCUSSION AND CONCLUSIONS

An improved parameterization for the transilient coefficients in which used a simplified form of the turbulent kinetic energy (TKE) equation has been presented in this paper. The second moment terms of the TKE equation are approximated by the first-order moment (mean) variables. The approach is still classified as a parameterization to the discrete form of transilient turbulence theory. The parameterization described above reduces the freedom degrees from $(N^2 - N)$ to four and the sensitivity of model has been studied using Qinhuangdao PBL data. The non-local closure scheme used in this 2-D model includes following contents: (1) because the turbulent exchange in upper and lower levels is non-uniform, it is imperimitive to use the non-uniform exchange coefficients by considering the normalization treatment on the TKE equation; (2) only the vertical non-local turbulent exchange is considered, for the order of the horizontal diffusion term is much smaller than advection term and can be omitted; (3) since the effects of horizontal advection are more evident that effects of horizontal diffusion should be considered especially under windy condition. Under ideal condition, the model was used to simulate TIBL and sea-land breeze circulation and the results were reasonable. The model was also used to prognose the fields of wind, potential temperature and fluxes using the data from field experiment in Qinhuangdao. The results were in good agreement with the field measurement.

REFERENCES

Blackadar, A. K. (1987), Modeling pollutant transfer during daytime convection, Preprints Fourth Symp. On Atmospheric Turbulence, Diffusion, and Air Quality, AMS Reno, NV. 443–447.

Clarke, R. H. et al. (1971), The Wangara Experiment-Boundary Layer Data, Paper No. 19 Division Meteorological Physics, CSIRO. Australia.

Jiang Weimei, Wang Yanchang and Zhong Shiyuan (1991), Observation study on wind in PBL and its transport and dispersion in coastal region, *Oceanologica ET Limnolgu Sinica*, **22**: 140–147.

McNider, R. T. (1981), Investigation of the input of topographic circulations on the transport and dispersion of air pollutants, Ph. D Dissertation.

McNider, R, T. and R. A. Pielke (1981), Diurnal bouncary-layer development over slopping terrain, *J. Atmos.*

Sci., **38**: 2198–2212.

Pielke, R. A. (1984), Mesoscale Meteorological Modeling, Academic Press, Orlando, 612 pp.

Stull, R. B. (1984), Transilient turbulence theory, Part 1: The concept of eddy mixing across finite distance, *J. Atmos. Sci.*, **41**: 3351–3367.

Stull, R. B. (1987), Transilient turbulence algorithms to model mixing across finite distances, *Environ. Software*, **2**: 4–12.

Stull, R. B. (1993), Review of non-local mixing in turbulent atmospheres: transilient turbulence theory, *Boundary-Layer Meteorology*, **62**: 21–96.

Wang Xuemei and Jiang Weimei (1993), The non-local closure model and its application in PBL, *J. Nanjing University (Natural Sciences)* **29**: 133–137.

Zhang, D. L. and Anthes, R. A. (1982), A high-resolution model of the planetary boundary layer–sensitivity tests and comparisons with SESAME-79 data, *J. Appl. Met.*, **21**: 1594–1606.